Volume 23
Number 36
28 September 2025
Pages 8065-8342

Organic & Biomolecular Chemistry

rsc.li/obc

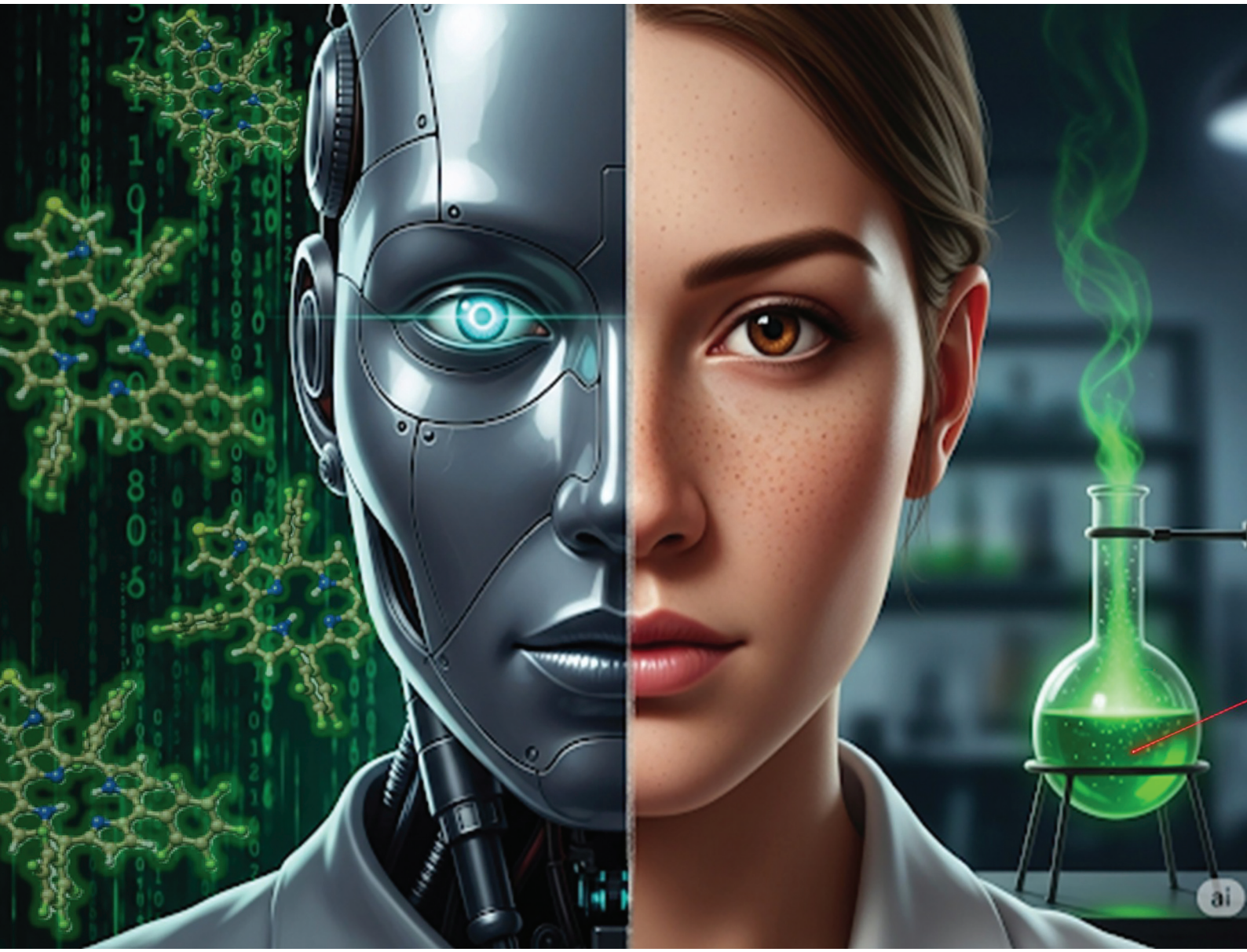

ISSN 1477-0520

ROYAL SOCIETY OF CHEMISTRY

PAPER

Giampaolo Barone, Ana M. G. Silva *et al.*
Sulphur-containing pyrrolidine-fused chlorins as potential candidates for photodynamic therapy: experimental and theoretical photophysical evaluation

Organic & Biomolecular Chemistry

ROYAL SOCIETY OF CHEMISTRY

PAPER

View Article Online
View Journal | View Issue

Check for updates

Cite this: *Org. Biomol. Chem.*, 2025, **23**, 8212

Sulphur-containing pyrrolidine-fused chlorins as potential candidates for photodynamic therapy: experimental and theoretical photophysical evaluation†

Juliana Machado, [a] José Almeida,[a] Tânia M. Ribeiro, [b] Tiago E. C. Magalhães, ‡[b] Valeria Butera,[c] Giampaolo Barone *[c] and Ana M. G. Silva *[d]

Two novel sulphur-containing pyrrolidine-fused chlorin derivatives, **Chlor-SH_*trans*** and **Chlor-CSH_*trans***, were synthesized through a 1,3-dipolar cycloaddition reaction of *meso*-tetrakis(pentafluorophenyl)porphyrin with azomethine ylides generated *in situ* through the condensation of paraformaldehyde with cysteine or L-thiazolidine-4-carboxylic acid (for **Chlor-SH_*trans***) and homocysteine (for **Chlor-CSH_*trans***). The synthesized chlorins were structurally characterized using various techniques, including nuclear magnetic resonance, UV-vis absorption and fluorescence spectroscopy and mass spectrometry. Density functional theory calculations confirmed that the *trans* isomer is the most stable for both chlorins, corroborating nuclear magnetic resonance findings. The reaction mechanisms were elucidated, revealing the potential formation of multiple products from the interaction of formaldehyde units with the amino acids cysteine or homocysteine. **Chlor-CSH_*trans*** exhibited enhanced stability, potentially due to the formation of a six-membered ring. In dimethylformamide, **Chlor-CSH_*trans*** demonstrated a slightly higher molar absorption coefficient at 650 nm, but a lower fluorescence quantum yield compared to **Chlor-SH_*trans***. Interestingly, **Chlor-SH_*trans*** showed enhanced singlet oxygen production, attributed to a higher value of spin–orbit coupling and higher triplet state stability. Neither chlorin exhibited significant aggregation or photodegradation at the studied concentrations, indicating promising properties for photodynamic applications.

Received 8th May 2025,
Accepted 8th July 2025

DOI: 10.1039/d5ob00753d

rsc.li/obc

Open Access Article. Published on 10 iyul 2025. Downloaded on 06.02.2026 22:33:51.
This article is licensed under a Creative Commons Attribution 3.0 Unported Licence.

Introduction

Photodynamic therapy (PDT) is a minimally invasive therapy that uses a photosensitizer (PS), molecular oxygen and light to induce cell death.[1] Initially developed for cancer treatment,[2] the application of PDT has since expanded to various medical fields, including dermatology,[3] ophthalmology,[4] and dentistry.[5] Additionally, PDT has demonstrated antimicrobial[6] and antiviral activities,[7] making it a potential treatment for infectious diseases.

Ideally, the PS should accumulate in cancer tissues or cells, thereby minimizing damage to healthy surrounding areas,[8–11] and preferentially target different subcellular organelles, including mitochondria, endoplasmic reticulum, and lysosomes. The PDT process initiates with the photoactivation of the PS, which involves the transition from its ground state to an electronically excited singlet state (Fig. 1). At this stage, due

[a]*LAQV-REQUIMTE, Departamento de Química e Bioquímica, Faculdade de Ciências, Universidade do Porto, 4169-007 Porto, Portugal*
[b]*Instituto de Física de Materiais Avançados, Nanotecnologia e Fotónica (IFIMUP), Departamento de Física e Astronomia, Faculdade de Ciências, Universidade do Porto, Rua do Campo Alegre s/n, 4169-007 Porto, Portugal*
[c]*Scienze e Tecnologie Biologiche Chimiche e Farmaceutiche, Università degli Studi di Palermo, Italy*
[d]*LAQV-REQUIMTE, Instituto de Ciências Biomédicas Abel Salazar da Universidade do Porto, Rua de Jorge Viterbo Ferreira, 228, 4050-313 Porto, Portugal*
†Electronic supplementary information (ESI) available. See DOI: https://doi.org/10.1039/d5ob00753d
‡Present address: INL – International Iberian Nanotechnology Laboratory, Av. Mestre José Veiga S/N, 4715–330 Braga, Portugal.

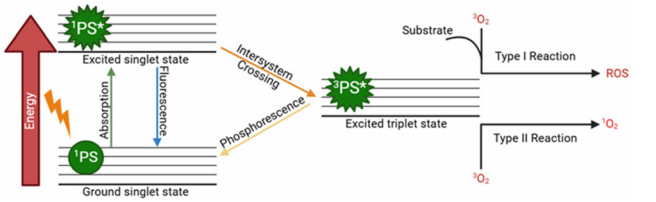

Fig. 1 Simplified Jablonski diagram for production of ROS through Type I and II mechanisms.

This journal is © The Royal Society of Chemistry 2025

Open Access Article. Published on 10 iyul 2025. Downloaded on 06.02.2026 22:33:51. This article is licensed under a Creative Commons Attribution 3.0 Unported Licence.

to its electronic structure, the PS can undergo intersystem crossing (ISC), leading to the transition to an excited triplet state. In this state, the PS can undergo two types of reaction pathways: (a) Type I involving an electron transfer to form radical intermediates or (b) Type II involving energy transfer to molecular oxygen to form singlet oxygen ($^1O_2$).[12–15] As a result, oxidative damage can occur, potentially leading to cell death through various pathways, including necrosis, apoptosis, and autophagy.[16,17]

In PDT, it is generally considered that Type II predominates over Type I, with $^1O_2$ standing out as the main cytotoxic agent responsible for the oxidation of various biologically important macromolecules, including nucleic acids, proteins, and lipids.[13] Although $^1O_2$ is highly reactive, it has a short lifetime and a small radius of diffusion, which limits its spread from the site of formation.[18]

PSs can be classified into three generations: (I) first-generation PSs, which include hematoporphyrin (Hp) and other porphyrin-based molecules characterized by light activation at wavelengths below 640 nm, exhibiting slow body clearance and prolonged skin photosensitivity;[17] (II) second-generation PSs, which include chlorin derivatives with improved cancer specificity and tissue penetration, absorption spectrum ranging from 650–800 nm (within the therapeutic window) and fewer side effects. However, many of these PSs have poor water solubility, which can result in aggregation in solution and low generation of singlet oxygen;[16] and (III) third-generation PSs, involving conjugation or encapsulation of second-generation PSs within a transport vehicle, thereby allowing the achievement of better stability and hydrophilicity, and enhanced pharmacokinetics, pharmacodynamics and biodistribution.[12]

Thus, the key characteristics of an ideal PS include: (i) absorption within the phototherapeutic window and a high molar extinction coefficient; (ii) efficient singlet oxygen production; (iii) high photostability and resistance to photodegradation during the irradiation process; (iv) selectivity for cancer cells or target tissue; (v) low dark toxicity; (vi) water solubility or compatibility with delivery systems; (vii) chemical purity and stability; and (viii) rapid clearance from the body.[12,19,20]

It has been reported that the combination of important features of both organic and inorganic PSs results in metal–organic dyads with extraordinary phototherapeutic and photocytotoxicities indices.[21–23] On the other hand, the search of organic compounds with unprecedented PDT activity is also growing.

Chlorins, which are hydroporphyrins, satisfy several criteria for ideal PSs. Notably, they have an intense absorption band around 650 nm, allowing for optimal tissue penetration of light during PDT treatment. Additionally, the introduction of heavy atoms into the PS's structure has been explored as a strategy to improve its triplet excited state population. This is crucial for the generation of ROS, particularly $^1O_2$, which is the primary cytotoxic agent in the PDT process. An interesting example of this strategy came from Prejanò *et al.*,[24] who demonstrated that replacing an oxygen atom with a sulphur in 4-dimethylaminonaphthalimide dyes results in a red shift of the Q absorption band and an increase in spin–orbit coupling (SOC) constants, suggesting a more efficient ISC mechanism. Furthermore, Tong *et al.*[25] showed that the addition of sulphur containing motifs to porphyrin could enhance both photodynamic and photothermal effects. Hence, the introduction of sulphur in PSs can potentially lead to a higher ability to produce $^1O_2$ and increased solubility of the PS.[26,27]

Inspired by these results, we decided to employ a 1,3-dipolar cycloaddition (1,3-DC) approach to synthesize sulphur-containing chlorins using *meso*-tetrakis(pentafluorophenyl) porphyrin (**TPFPP**) and azomethine ylides, generated *in situ* through the condensation of paraformaldehyde with cysteine or L-thiazolidine-4-carboxylic acid and homocysteine. Synthesis optimization was conducted using microwave heating, which provides higher heat transfer efficiency and improved heat distribution.[28] The potential application of these two chlorins in PDT was explored through UV-Vis spectroscopy, fluorescence quantum yield measurements, singlet oxygen generation and photostability assays, and DFT calculations.

Results and discussion

Synthesis

1,3-DCs are highly versatile, regio- and stereoselective reactions that have consistently drawn the attention of organic chemists due to their ability to construct diverse five-membered heterocycles. In porphyrin chemistry, these reactions have been extensively employed to synthesize chlorins fused to various heterocyclic rings. Many of these chlorin derivatives exhibit promising photophysical and biological properties, making them potential candidates for PDT.[29–33]

meso-Tetrakis(pentafluorophenyl)porphyrin (**TPFPP**) stands out as one of the most reactive porphyrins, acting as a dipolarophile in 1,3-DC reactions.[29] Its high reactivity is primarily attributed to the strong electron-withdrawing pentafluorophenyl groups at the *meso* positions of the macrocycle. Regarding 1,3-dipoles, azomethine ylides, which contain four π electrons distributed over a C–N–C group, have been widely investigated.[32] A straightforward approach involves reacting **TPFPP** with the azomethine ylide generated *in situ* from sarcosine and paraformaldehyde to yield *N*-methyl pyrrolidine-fused chlorin as a single product (Fig. 2a).[29] The complexity of these reactions increases when substituents are introduced at the terminal positions of the azomethine ylide, leading to the formation of *endo*/*exo* diastereoisomeric chlorins (Fig. 2b). Specifically, while the *N*-methyl pyrrolidine-fused chlorin is a *meso* compound, the newly synthesized sulphur-containing chlorins yield a mixture of two distinct *endo*/*exo* diastereoisomers. Each of these diastereoisomers is present as a racemic mixture. This stereochemical outcome is directly determined by the structure of the azomethine ylide used in the reaction.

Following this line of research, we used cysteine, L-thiazolidine-4-carboxylic acid and homocysteine to generate the 1,3-dipole, with the aim of studying the reaction products

Open Access Article. Published on 10 iyul 2025. Downloaded on 06.02.2026 22:33:51.
This article is licensed under a Creative Commons Attribution 3.0 Unported Licence.

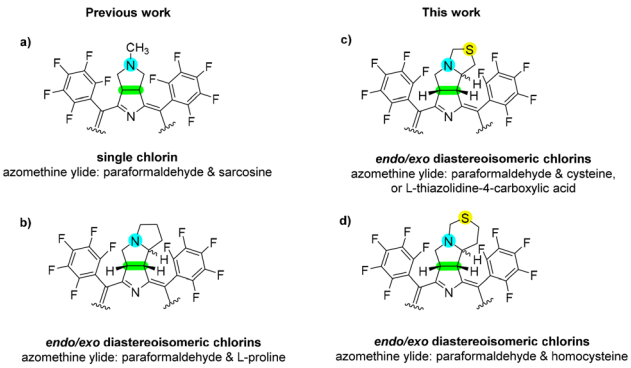

Fig. 2 Single chlorin (a) and diastereoisomeric chlorins (b–d) obtained from 1,3-DC reactions.[29]

and evaluating their potential activity as PSs for PDT (Fig. 2c and d).

Our initial studies involved a 1,3-DC between **TPFPP** and the azomethine ylide generated *in situ* from cysteine and paraformaldehyde in a 5 : 5 molar ratio (Scheme 1a). The reaction, conducted under conventional heating for 8 hours, yielded two distinct fractions upon column chromatography: recovered **TPFPP** (82%) and **Chlor-SH_*trans*** (7%). Although minor secondary products were observed, **Chlor-SH_*trans*** was isolated as the main product and subsequently characterized, and its photophysical properties were evaluated. To improve the efficiency of the reaction, modifications to the original protocol were made based on previous work involving the 1,3-DC approach.[34,35] Notably, the use of microwave (MW) irradiation successfully reduced the reaction time from 8 hours to 2 hours, representing a significant decrease in reaction time. For these reactions, chlorobenzene was chosen as the solvent due to its high dielectric constant, making it more suitable for microwave-assisted synthesis.

A second approach for the synthesis of **Chlor-SH_*trans*** was developed using a 1,3-DC between **TPFPP** and the azomethine ylide generated from L-thiazolidine-4-carboxylic acid and paraformaldehyde (Scheme 1b). According to both theoretical and experimental studies (*vide infra*), L-thiazolidine-4-carboxylic acid is the major product of the reaction between cysteine and paraformaldehyde. This compound can further react with paraformaldehyde to form the 1,3-dipolar species. The use of L-thiazolidine-4-carboxylic acid as a precursor may offer potential advantages in terms of reaction efficiency and product formation, potentially providing a more direct route for the synthesis of the desired 1,3-dipolar species and reducing side reactions. Using this approach, **Chlor-SH_*trans*** was obtained in 9% yield, which is slightly higher than that obtained with the initial method. Furthermore, 73% of **TPFPP** was recovered, allowing for its potential reuse in subsequent 1,3-DC reactions to increase product yield (Table S5†).

Using a similar approach, **Chlor-CSH_*trans*** was synthesised through a 1,3-DC between **TPFPP** and the azomethine ylide generated from homocysteine and paraformaldehyde in a 5 : 5 molar ratio (Scheme 2). The reaction was carried out under conventional heating conditions for 8 hours and purified by column chromatography, resulting in four distinct fractions: recovered **TPFPP** (62%), **Chlor-CSH_*trans*** (22%), and two minor fractions corresponding to a bisadduct and a second chlorin named **Chlor-CSH_*cis***. Other secondary products were observed, but in very small amounts. Also in this case, the use of MW irradiation successfully reduced the reaction time from 8 hours to 2 hours, representing a significant improvement in the synthetic procedure. Other experimental conditions were explored, including: (i) increasing the concentrations of reagents and (ii) lowering the reaction temperature (Table S5†). However, neither of these approaches proved successful in enhancing the yield of **Chlor-CSH_*trans***. Notably, the use of homocysteine instead of cysteine resulted in a higher yield of **Chlor-CSH_*trans*** (21–22%) compared to the synthesis of **Chlor-SH_*trans*** (6–9%). This suggests that the longer carbon chain of homocysteine may favourably influence the reaction outcome.

The structures of **Chlor-SH_*trans*** and **Chlor-CSH_*trans*** were confirmed by NMR spectroscopy (Fig. S1–S12†) as well as by ESI mass spectrometry (Fig. S14 and S15†). In the ^{1}H NMR spectrum of **Chlor-SH_*trans*** (Fig. S1†), the triplet signal appearing at 3.72 ppm is attributed to the H-2^{3a} proton (J = 8.4 Hz). In the COSY spectrum (Fig. S4†), this signal shows cross-peaks with two double doublets at 2.75 and 2.86 ppm attributed to H-2^3 *cis* and *trans*, while no cross-peaks were observed with H-3. This reveals a *trans* configuration between H-2^{3a} and H-3, possibly related to a dihedral angle approaching 90°,

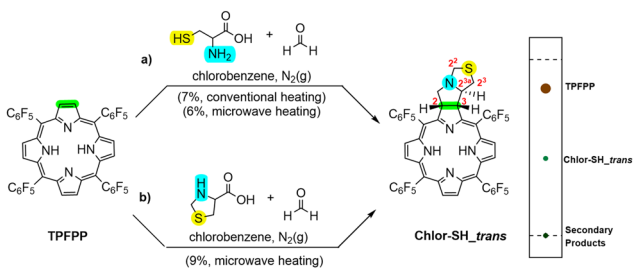

Scheme 1 Synthesis of **Chlor-SH-*trans*** through 1,3-DC of **TPFPP** and azomethine ylide generated from paraformaldehyde and (a) cysteine and (b) L-thiazolidine-4-carboxylic acid. TLC representation of the reaction mixture eluted with a mixture of hexane/dichloromethane (6 : 4).

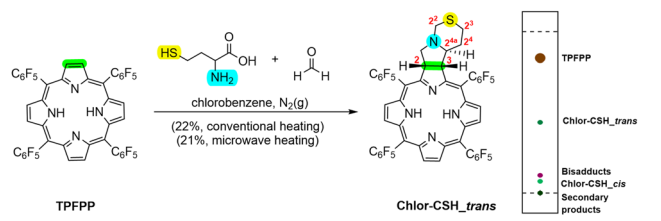

Scheme 2 Synthesis of **Chlor-CSH_*trans*** through 1,3-DC of **TPFPP** and azomethine ylide generated from paraformaldehyde and homocysteine. TLC representation of the reaction mixture eluted with a mixture of hexane/dichloromethane (6 : 4).

This journal is © The Royal Society of Chemistry 2025

Open Access Article. Published on 10 iyul 2025. Downloaded on 06.02.2026 22:33:51.
This article is licensed under a Creative Commons Attribution 3.0 Unported Licence.

which is in agreement with theoretical predictions (*vide infra*). In the HSQC spectrum (Fig. S5†), H-2[3a] correlates with the more deshielded aliphatic carbon signal at 77.2 ppm, allowing the unequivocal attribution of this signal to C-2[3a].

For **Chlor-CSH_*trans*** (Fig. S7†), the H-2[4a] proton appears as a double doublet at 3.49 ppm (J = 12.4 and J = 3.2 Hz), which shows COSY (Fig. S10†) cross-peaks with the signals corresponding to H-2[4] *cis* and *trans*. However, no cross-peak is observed between H-2[4a] and H-3. This spectroscopic evidence indicates a *trans* configuration between H-2[4a] and H-3, which is supported by theoretical calculations (*vide infra*). In the HSQC spectrum (Fig. S11†), H-2[4a] correlates with the more deshielded aliphatic carbon signal at 65.6 ppm, allowing the unequivocal attribution of this signal to C-2[4a].

Regarding the ^{19}F NMR spectra (Fig. S3 and S9†), no alterations in the signals were observed compared with the starting porphyrin (**TPFPP**), confirming the integrity of the pentafluorophenyl groups at the *meso* positions of both chlorins.

DFT calculations

Thermodynamic calculations were performed for all reaction steps leading to the formation of sulphur-containing pyrrolidine-fused chlorins, considering both *cis* and *trans* configurations (Tables S2 and S3†), using eqn (1) (see *infra*).

When combining an amino acid and formaldehyde, three different products can form: (a) azomethine ylide **1** (Scheme S1a†), (b) a thermodynamic product (Scheme S1b†), and (c) a kinetic product (Scheme S1c†).[36] The thermodynamic product can further react with paraformaldehyde and form another 1,3-dipolar species, azomethine ylide **2** (Scheme S2†). For the formation of the azomethine ylide **1**, a ΔG_f° value of 7.2 kJ mol^{-1} and 13.6 kJ mol^{-1} was obtained in the reaction of paraformaldehyde with cysteine and homocysteine, respectively (Table S2 and Fig. S17†). For the formation of azomethine ylide **2**, a ΔG_f° value of 4.8 kJ mol^{-1} and 104.2 kJ mol^{-1} was obtained in the reaction of paraformaldehyde with L-thiazolidine-4-carboxylic acid and 1,3-thiazinane-4-carboxylic acid, respectively (Table S3 and Fig. S18†). In the case of the reaction of 1,3-thiazinane-4-carboxylic acid (thermodynamic product) with paraformaldehyde, the high ΔG_f° value indicates an unlikeliness of the formation of this product, and a conclusion that only the pathway involving the azomethine ylide **1** can occur.

However, for forming **Chlor-SH**, two different pathways can occur simultaneously, which explains the slight improvement in experimental yield when starting from L-thiazolidine-4-carboxylic acid (thermodynamic product) since the formation of the kinetic product would not occur in this case. Thus, the two possible pathways are: (i) 1,3-DC of **TPFPP** with azomethine ylide **1**, followed by reaction with another formaldehyde molecule, leading to the formation of the second ring or (ii) 1,3-DC of azomethine ylide **2** with **TPFPP** (Scheme 3).

As is well known, the porphyrin ring system, due to its planarity, creates two different faces that the azomethine ylide can approach, leading to *endo* or *exo* stereoisomers.[37] Kinetic studies of the 1,3-DC reaction of pathway 1 performed for

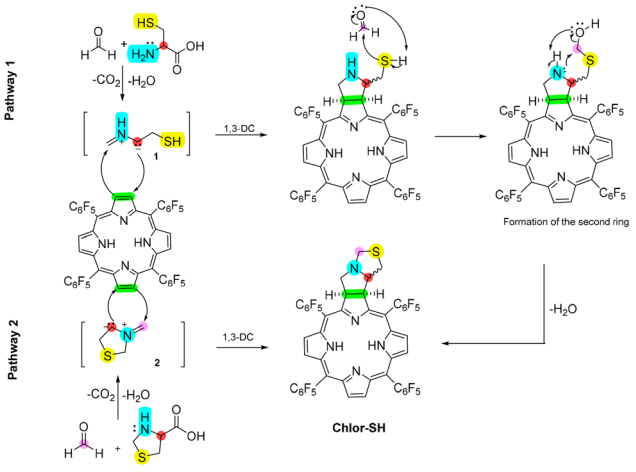

Scheme 3 Two possible pathways for the synthesis of **Chlor-SH** through 1,3-DC of **TPFPP** and azomethine ylide generated from paraformaldehyde and cysteine (Pathway 1) or L-thiazolidine-4-carboxylic acid (Pathway 2).

Chlor-SH show the approximation of the 1,3-dipolar species in an *endo* and *exo* approach, giving rise to **Chlor-SH_*trans*** and **Chlor-SH_*cis***, respectively (Fig. S19†). Finally, in pathway 1, the reaction with formaldehyde occurs spontaneously (shown by the negative values of ΔG_f) for both isomers for **Chlor-SH** and **Chlor-CSH**.

In both reactions, the *trans* isomer (−51.9 and −70.3 kJ mol^{-1}, respectively) has a higher stability than the *cis* isomer (−50.9 and −63.0 kJ mol^{-1}), as shown by a more negative relative Gibbs free energy value. By comparing the formation energy of **Chlor-SH_*trans*** (−181.5 kJ mol^{-1}) and **Chlor-CSH_*trans*** (−193.5 kJ mol^{-1}), it is possible to conclude that **Chlor-CSH_*trans*** is more stable, having a lower ΔG_f, possibly due to the formation of the six-membered ring, and this can be related to its higher yield (Fig. 3a and Table S2†).

Furthermore, the analysis of the linear correlation between theoretical *vs.* experimental ^{1}H and ^{13}C NMR chemical shift values (Table S4, Fig. S20 and S21†) shows a higher linear cor-

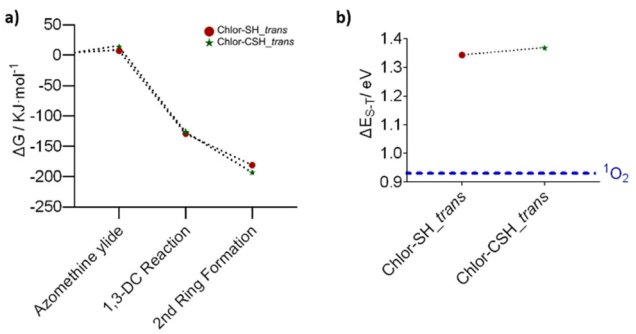

Fig. 3 (a) Standard Gibbs free energy of formation values, relative to the reactants, for **Chlor-CSH_*trans*** and **Chlor-SH_*trans***, calculated using eqn (2) and (b) energy difference between the ground singlet state and the excited triplet state, calculated using eqn (3).

Open Access Article. Published on 10 iyul 2025. Downloaded on 06.02.2026 22:33:51.
This article is licensed under a Creative Commons Attribution 3.0 Unported Licence.

relation coefficient R^2 for the *trans* isomer for both chlorins, corroborating the structural attributions by NMR spectroscopy.

The computed energy required to generate the singlet oxygen species is 0.93 eV,[38] which is in good agreement with the experimental value of 0.98 eV. The singlet–triplet energy gap (ΔE_{S-T}) calculated for **Chlor-SH_*trans*** (1.34 eV) and **Chlor-CSH_*trans*** (1.37 eV) is larger than the ΔE_{S-T} of oxygen, showing that both compounds have the ability to promote the formation of singlet oxygen. Furthermore, the triplet state of **Chlor-SH_*trans*** is more stable than that of **Chlor-CSH_*trans***, suggesting a longer triplet state lifetime, resulting in higher singlet oxygen production (Fig. 3b).

For both chlorins, there are two triplet states below the first singlet and one triplet is close in energy to the singlet, leading to three possible ISC channels (Table 1). The spin–orbit coupling (SOC) values were calculated. Our results show a higher value of SOC for **Chlor-SH_*trans*** for all the channels, which should result in higher singlet oxygen production, as shown in the experimental results (see *infra*).

Study of optical properties

UV-Vis spectroscopy. The electronic spectra of chlorins were obtained at different concentrations. Absorbance was studied as a function of concentration at the maximum absorption wavelength (λ_{max}) of the Soret and Q-bands. The slope from the linear fitting corresponds to the molar absorption coefficient (ε), according to the Lambert–Beer law ($A = \varepsilon\, l\, c$, with A being the absorbance, l the path-length and c the concentration).[39] A higher molar extinction coefficient shows a higher absorbance by the chlorin. Hence, at 652 nm (band at the photodynamic window), **Chlor-CSH_*trans*** shows a relatively higher absorption capability than **Chlor-SH_*trans*** (Table 2).

Since most porphyrins and chlorins have a great tendency to self-aggregate, due to stacking from interaction between π-systems,[40] which can reduce singlet oxygen generation and lower PDT capabilities, the prepared solutions were used to study the tendency of aggregation of chlorins in DMF (Fig. S23 and S24†). The results obtained show a linear relationship between absorbance and concentration, following the Lambert–Beer law. Moreover, λ_{max} and band broadening remained stable over the range of concentrations studied for both chlorins in DMF at room temperature. This tendency can be extrapolated to lower concentrations, since the aggregation phenomenon increases with the increase in concentrations. The asymmetry of the chlorins can be the reason for the reduced aggregation.[41]

We have also assessed the stability in solution over time of both chlorins **Chlor-SH_*trans*** and **Chlor_CSH_*trans***, which demonstrated that these compounds remain stable in DMF solution for at least one year (Fig. S25 and S26†).

Fluorescence quantum yield measurements. When exposed to light, chlorins can absorb energy and become excited. The subsequent de-excitation process can happen *via* fluorescence or phosphorescence. The fluorescence of chlorins is characterized by an emission at around 655 nm, as is shown for the synthesized chlorins (Fig. S27†). As shown in Fig. 4, the fluorescence quantum yield (Φ) of both **Chlor-SH_*trans*** and **Chlor-CSH_*trans*** is moderately solvent dependent. These compounds display higher Φ values in low-polarity solvents like toluene (ε = 2.38) compared to polar solvents such as methanol (ε = 32.7) and DMF (ε = 36.7). This trend suggests that the fluorescence efficiency decreases with increasing solvent polarity, likely due to enhanced non-radiative decay pathways in polar environments. Notably, **Chlor-CSH_*trans*** in DMF exhibits the

Table 1 SOC values (cm^{-1}) of the more relevant ISC channels from S_n to T_m of **Chlor-SH_*trans*** and **Chlor-CSH_*trans*** and the corresponding energy gap $\Delta E(S_n–T_m)$ (eV)

Chlor-SH_*trans*			**Chlor-CSH_*trans***		
$S_n–T_m$	SOC($S_n–T_m$)	$\Delta E(S_n–T_m)$	$S_n–T_m$	SOC ($S_n–T_m$)	$\Delta E(S_n–T_m)$
$S_1–T_1$	5.09	0.34	$S_1–T_1$	3.63	0.29
$S_1–T_2$	4.15	0.33	$S_1–T_2$	0.88	0.28
$S_1–T_3$	2.06	−0.01	$S_1–T_3$	1.98	−0.01

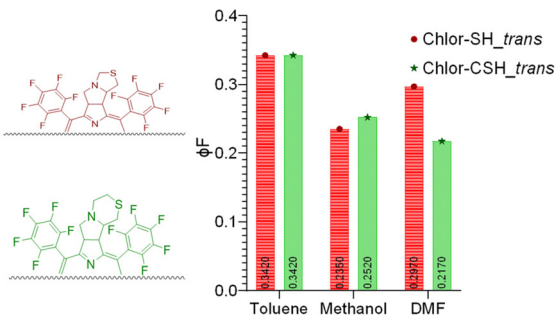

Fig. 4 Graphical representation and values obtained for fluorescence quantum yields (Φ) of **Chlor-SH_*trans*** and **Chlor-CSH_*trans*** in toluene, methanol and DMF.

Table 2 Molar extinction coefficient of the absorption bands for **Chlor-SH_*trans*** and **Chlor-CSH_*trans*** in DMF solutions at 25 °C

	Absorption			
	λ_{max} nm^{-1} (ε/mol^{-1} dm^{-3} cm^{-1})			
Chlorin	Soret		Q bands	
Chlor-SH_*trans*	405 (1.32×10^5)	503 (1.23×10^4)	598 (3.99×10^3)	652 (3.34×10^4)
Chlor-CSH_*trans*	406 (1.35×10^5)	504 (1.28×10^4)	598 (3.99×10^3)	652 (3.66×10^4)

This journal is © The Royal Society of Chemistry 2025

Open Access Article. Published on 10 iyul 2025. Downloaded on 06.02.2026 22:33:51.
This article is licensed under a Creative Commons Attribution 3.0 Unported Licence.

lowest quantum yield, aligning with the observed inverse relationship between Φ and dielectric constant.

Singlet oxygen assay. Singlet oxygen is known as the major cytotoxic agent of PDT. For its measurement, we employed a spectroscopic method, using 1,3-diphenylbenzofuran (DPiBF) as the probe, which exhibits a characteristic absorbance band at 415 nm. This compound can react with $^1O_2$ and other ROS species to form an endoperoxide *via* a [4 + 2] cycloaddition, which subsequently decomposes into 1,2-dibenzoylbenzene, resulting in loss of absorbance at 415 nm.[42] Since **Chlor-CSH_*trans*** has a lower fluorescence quantum yield in DMF, it might be expected to be the one with higher production of $^1O_2$. However, as shown in Fig. 5, **Chlor-SH_*trans*** showed the best performance. When compared with the theoretical data obtained, **Chlor-SH_*trans*** showed a lower ΔG between singlet and triplet states and higher values of SOC, which could indicate a higher triplet quantum yield and lifetime and explain the higher values of singlet oxygen production.

Photostability assay. Photostability studies were performed using an adaptation of the method described by N. Moura *et al.*[43] The chlorin samples were irradiated for 30 min using a halogen lamp with an irradiance of 40 mW cm^{-2}. The UV-Vis spectra, recorded at 5 min intervals, did not show any signs of degradation, as the absorption bands maintained their absorbance over time for both chlorins **Chlor-SH_*trans*** and **Chlor-CSH_*trans*** (Fig. S28 and S29†).

Experimental

Materials and methods

All reagents and solvents were of reagent-grade and used with no additional purification unless otherwise stated.

Flash chromatography was accomplished using silica gel (Merck, 230–400 mesh), while preparative thin-layer chromatography (TLC) was performed on 20 × 20 cm glass plates coated with Merck 60 silica gel (1 mm thick). Analytical TLC was performed on silica gel precoated sheets (Merck 60, 0.2 mm thickness).

Microwave-mediated cycloaddition reactions were carried out in a CEM Discovery Labmate circular single-mode cavity instrument (300 W max magnetron power output) from CEM Corporation.

High-resolution mass spectrometry (HRMS) analysis was performed *via* electrospray ionization (ESI) using an LTQ-Orbitrap-XL instrument (Thermo Scientific) with the following ESI source parameters: electrospray needle voltage, 3.1 kV; sheath gas (nitrogen), 6; capillary temperature, 275 °C; capillary voltage, 41 V and tube lens voltage, 130 V. Ionization polarity was adjusted according to the sample.

Nuclear magnetic resonance (NMR) spectra for all compounds were recorded on a 400 MHz NMR spectrometer (operating at 400.14 MHz for proton, 100.62 MHz for carbon and 376.52 MHz for fluorine atoms), where $CDCl_3$ was used as the solvent and TMS as the internal reference. The chemical shifts (δ) are expressed in ppm and the coupling constants (J) in Hz. In the case of ^{19}F NMR spectra, $C_6H_5CF_3$ was used as the reference.

Electronic absorption spectra were recorded on a Shimadzu UV-3600 UV-Vis-NIR spectrophotometer, equipped with a Shimadzu TCC-Controller (TCC-240A), at 25 °C, in 1 cm path length cuvettes, in the wavelength range of 300–800 nm. The solutions were prepared in DMF in concentration ranges of 10^{-5}–10^{-7} mol dm^{-3} for the determination of the molar absorption coefficient (ε). Six valid values for each absorption band (below 1 of absorbance) were obtained. The λ_{max} for each band and the broadness of the band were recorded and compared to evaluate possible aggregations.

Fluorescence measurements were performed in a Varian Cary Eclipse fluorimeter, equipped with a constant temperature cell holder (Peltier single cell holder), at 25 °C, in 1.00 cm cuvettes. Spectra were recorded with excitation and emission slit widths between 5 and 10 nm and 650 to 700 V. Emission spectra were recorded by exciting the corresponding absorption λ_{max} of each chlorin. To minimize reabsorption effects, sample's absorbance values were kept below 0.1. The solutions for the fluorescence measurements were prepared in DMSO and diluted with the studied solvent, with the final concentration of DMSO being below 2%. Absolute photoluminescence quantum yield measurements were carried out using an absolute photoluminescence quantum yield spectrometer (Quantaurus QY C11347-11 spectrometer) equipped with an integrating sphere to measure all the luminous flux, using a stock solution of chlorin in DMSO, which was dissolved in the desired solvent to obtain a solution with absorbance values below 0.1.

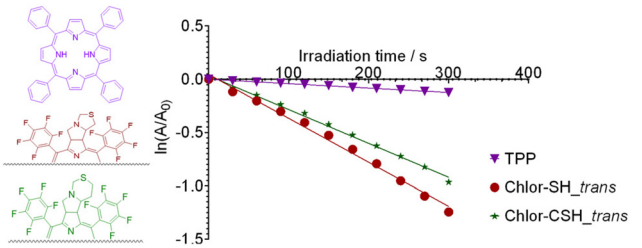

Fig. 5 Singlet oxygen generation of **TPP** (purple), **Chlor-SH_*trans*** (red) and **Chlor-CSH_*trans*** (green) by monitoring the decrease in the absorbance of DPiBF at 415 nm in DMF under red-light irradiation at 30 seconds intervals, represented by the linear regression of $\ln(A/A_0)$ as a function of irradiation time. **TPP** (purple) was used as the reference photosensitizer.

Synthetic procedures

The synthesis of *meso*-tetrakis(pentafluorophenyl)porphyrin (**TPFPP**) was carried out using the method described by A. M. d'A Rocha Gonsalves *et al.*[44]

Synthesis of Chlor-SH_*trans*

Under conventional heating. TPFPP (40.0 mg, 4.10 × 10^{-5} mol) was dissolved in 5 mL of chlorobenzene. In a mortar, cysteine (24.9 mg, 2.05 × 10^{-4} mol, 5 equiv.) and paraformaldehyde (6.2 mg, 2.05 × 10^{-4} mol, 5 equiv.) were ground together.

Open Access Article. Published on 10 iyul 2025. Downloaded on 06.02.2026 22:33:51. This article is licensed under a Creative Commons Attribution 3.0 Unported Licence.

Then, 9.0 mg of this mixture was added to the **TPFPP** solution. The reaction was performed in a conventional oil-bath, under an N_2 atmosphere and reflux conditions for 2 h. Three more additions of 9.0 mg of the cysteine/paraformaldehyde mixture were made, followed by another 2 h of reflux reaction cycle, resulting in a total reaction time of 8 h. After reaction completion, chlorobenzene was evaporated, and the reaction mixture was dissolved in dichloromethane and purified by flash chromatography using the following eluents: (i) a 6 : 4 mixture of hexane/dichloromethane to recover the remaining **TPFPP** (32.8 mg, 82% recovery) and (ii) a 1 : 1 mixture of hexane/dichloromethane to elute **Chlor-SH_*trans*** (3.0 mg; 7% yield).

Under microwave heating. TPFPP (40.0 mg, 4.10×10^{-5} mol) was dissolved in 5 mL of chlorobenzene. In a mortar, cysteine (24.9 mg, 2.05×10^{-4} mol, 5 equiv.) and paraformaldehyde (6.2 mg, 2.05×10^{-4} mol, 5 equiv.) were ground together and added to the **TPFPP** mixture. The reaction was performed under microwave heating conditions in an open vessel (135 °C and 290 W maximum power) for 2 h. After purification, using a similar work-up as described above, **Chlor-SH_*trans*** was obtained in 6% yield (2.7 mg) and 81% of **TPFPP** was recovered (32.4 mg).

Using L-thiazolidine-4-carboxylic acid. TPFPP (40.0 mg, 4.10×10^{-5} mol) was dissolved in 5 mL of chlorobenzene. In a mortar, L-thiazolidine-4-carboxylic acid (27.3 mg, 2.05×10^{-4} mol, 5 equiv.) and paraformaldehyde (6.2 mg, 2.05×10^{-4} mol, 5 equiv.) were ground together and added to the **TPFPP** mixture. The reaction was performed under microwave heating conditions in an open vessel (135 °C and 290 W maximum power) for 2 h. After purification, using a similar work-up as described above, **Chlor-SH_*trans*** was obtained in 9% yield (4.1 mg) and 73% of **TPFPP** was recovered (29.2 mg).

Chlor-SH_*trans*. ^{1}H NMR ($CDCl_3$, 400.14 MHz) δ = −1.73 (s, 2H, NH), 2.75 (dd, J = 7.6 and 10.0 Hz, 1H, H-2^3), 2.86 (dd, J = 9.6 and 10.0 Hz, 1H, H-2^3), 3.24 (d, J = 9.6 Hz, 1H, H-2^1), 3.31 (dd, J = 7.6 and 10.0 Hz, 1H, H-2^1), 3.72 (t, J = 8.4 Hz, 1H, H-2^{3a}), 3.94 and 3.99 (2d, J = 10.0 Hz, 2H, H-2^2), 5.28 (d, J = 8.2 Hz, 1H, H-3), 5.36 (dd, J = 7.6 and 8.2 Hz, 1H, H-2), 8.39 (d, J = 4.0 Hz, 2H, H-*β*), 8.47 (s, 2H, H-*β*), 8.70 (d, J = 5.0 Hz, 2H, H-*β*) ppm. **^{19}F{^{1}H} NMR ($CDCl_3$, 376.52 MHz)** δ = −161.23 to −161.75 (m, 4F, F_{meta}–Ar), −159.88 (ddd, J = 44.9, 21.1, 8.5 Hz, 2F, F_{meta}–Ar), −159.41 to −159.64 (m, 1F, F_{meta}–Ar), −159.07 to −159.30 (m, 1F, F_{meta}–Ar), −151.67 (t, J = 20.7 Hz, 2F, F_{para}–Ar), −151.06 (t, J = 20.9 Hz, 1F, F_{para}–Ar), −150.61 (t, J = 21.0 Hz, 1F, F_{para}–Ar), −137.60 (dd, J = 24.0, 8.2 Hz, 1F, F_{ortho}–Ar), −137.13 (dd, J = 24.2, 8.2 Hz, 1F, F_{ortho}–Ar), −136.88 to −137.05 (m, 2F, F_{ortho}–Ar), −136.57 to −136.86 (m, 2F, F_{ortho}–Ar), −134.51 (dd, J = 25.0, 7.4 Hz, 1F, F_{ortho}–Ar), −134.25 (dd, J = 24.1, 8.3 Hz, 1F, F_{ortho}–Ar) ppm. **^{13}C{^{1}H} NMR ($CDCl_3$, 100.62 MHz)** δ = 36.4 (C-2^3), 51.8 (C-2), 56.4 (C-2^1), 57.0 (C-3^1), 58.5 (C-2^2), 77.2 (C-2^{3a}), 96.6, 96.7,106.3, 106.4, 115.4, 115.6, 116.0, 123.7, 123.9,128.0, 128.1, 132.4, 132.5, 135.3, 135.3, 140,3. 140.6, 145.0, 147.5, 152.9, 152.9, 167.6, 169.2 ppm. **UV-Vis (DMF)** λ_{max} (log ε): 405 (5.12), 503 (4.09), 598 (3.60), 652 (4.61) nm. **Fluorescence (DMF)** λ_{max} = 655; 713 nm, ϕF = 0.297. **HRMS (ESI)** m/z: $[M + H]^+$ calculated for $C_{48}H_{18}F_{20}N_5S^+$ 1076.096 Da; found 1076.098 Da.

Synthesis of Chlor-CSH_*trans*

Under conventional heating. TPFPP (40.0 mg, 4.10×10^{-5} mol) was dissolved in 5 mL of chlorobenzene. In a mortar, homocysteine (27.7 mg, 2.05×10^{-4} mol, 5 equiv.) and paraformaldehyde (6.2 mg, 2.05×10^{-4} mol, 5 equiv.) were ground together. Then, 9.0 mg of this mixture was added to the **TPFPP** solution. The reaction was performed in a conventional oil-bath, under an N_2 atmosphere and reflux conditions for 2 h. Three more additions of 9.0 mg of the homocysteine/paraformaldehyde mixture were made, followed by another 2 h of reflux reaction cycle, for a total reaction time of 8 h. After reaction completion, chlorobenzene was evaporated, and the reaction mixture was dissolved in dichloromethane and purified by flash chromatography using the following eluents: (i) a 6 : 4 mixture of hexane/dichloromethane to recover the remaining **TPFPP** (24.7 mg, 62% recovered), (ii) a 1 : 1 mixture of hexane/dichloromethane to elute **Chlor-CSH_*trans*** (9.8 mg; 22% yield), and (iii) dichloromethane to elute a bisadduct and **Chlor-CSH_*cis*** (both obtained in very small amounts).

Under microwave heating. TPFPP (40 mg, 4.10×10^{-5} mol) was dissolved in 5 mL of chlorobenzene. In a mortar, homocysteine (27.7 mg, 2.05×10^{-4} mol, 5 equiv.) and paraformaldehyde (6.2 mg, 2.05×10^{-4} mol, 5 equiv.) were ground together and added to the **TPFPP** solution. The reaction was performed in a MW reactor under closed vessel conditions and an N_2 atmosphere (135 °C and 290 W maximum power) for 2 h. After purification, using a similar work-up as described above, the **Chlor-CSH_*trans*** was obtained in 21% yield (9.6 mg) and 62% of **TPFPP** was recovered (24.9 mg).

Chlor-CSH_*trans*. ^{1}H NMR ($CDCl_3$, 400.14 MHz) δ = −1.80 (s, 2H, NH), 0.88–0.93 and 1.88–1.99 (2m, 2H, H-2^4*cis* and *trans*), 2.73–2.78 (m, 2H, H-2^3), 2.99 (d, 1H, J = 10.0 Hz, H-2^1), 3.49 (dd, J = 12.4 and 3.2 Hz, 1H, H-2^{4a}), 3.60 (dd, J = 13.7 and 2.0 Hz, 1H, H-2^2), 3.97 (t, J = 9.0 Hz, 1H, H-2^1), 4.17 (d, J = 13.7 Hz, 1H, H-2^2), 4.78 (d, J = 8.4 Hz, 1H, H-3), 5.26 (t, J = 8.2 Hz, 1H, H-2), 8.38 (m, 2H, H-*β*), 8.46 (s, 2H, H-*β*), 8.69 (d, J = 4.9 Hz, 2H, H-*β*) ppm. **^{19}F{^{1}H}NMR ($CDCl_3$, 376.52 MHz)** δ = −161.54 (t, J = 18.3 Hz, 4F, F_{meta}–Ar), −160.47 to −160.67 (m, 1F, F_{meta}–Ar), −160.00 to −160.19 (m,1F, F_{meta}–Ar), −159.61 to −159.95 (m, 2F, F_{meta}–Ar), −151.78 (t, J = 21.0 Hz, 2F, F_{para}–Ar), −151.25 (t, J = 21.0 Hz, 1F, F_{para}–Ar), −151.00 (t, J = 21.0 Hz, 1F, F_{para}–Ar), −137.59 (dd, J = 24.0, 8.0 Hz, 1F, F_{ortho}–Ar), −137.10 (d, J = 8.9 Hz, 1F, F_{ortho}–Ar), −136.90 to −137.04 (m, 2F, F_{ortho}–Ar), −136.82 (d, J = 8.5 Hz, 1F, F_{ortho}–Ar), −136.76 (d, J = 8.5 Hz, 1F, F_{ortho}–Ar), −134.68 (dd, J = 23.7, 7.6 Hz, 1F, F_{ortho}–Ar), −134.28 (dd, J = 23.9, 6.1 Hz, 1F, F_{ortho}–Ar) ppm. **^{13}C{^{1}H}NMR ($CDCl_3$, 100.62 MHz)** δ = 25.6 (C-2^4), 27.1 (C-2^3), 28.7, 29.9, 49.5 (C-2), 51.2 (C-2^2), 52.4 (C-2^1), 57.8 (C-3), 65.6 (C-2^{4a}), 95.5, 95.7, 105.1, 114.4, 122.6, 122.8, 126.9, 127.0, 131.2, 134.2, 134.2, 139.3, 139.5, 144.0, 146.4, 151.7, 151.8, 167.9, 169.5 ppm. **UV-Vis (DMF)** λ_{max} (log ε): 406 (5.13), 503 (4.11), 598 (3.60), 652 (4.56) nm. **Fluorescence (DMF)** λ_{max} = 657;

 This journal is © The Royal Society of Chemistry 2025

Open Access Article. Published on 10 iyul 2025. Downloaded on 06.02.2026 22:33:51. This article is licensed under a Creative Commons Attribution 3.0 Unported Licence.

717 nm, ϕF = 0.217. **HRMS (ESI)** *m*/*z*: $[M + H]^+$ Calculated for $C_{49}H_{20}F_{20}N_5S^+$ 1090.1115 Da; found 1090.1109 Da.

Chlor-CSH_*cis*. ^{1}H NMR ($CDCl_3$, 400.14 MHz) δ = −1.72 (s, 2H, NH), 0.15–0.25 and 0.32–0.36 (2m, 2H), 1.91 (dd, *J* = 13.6 and 2.8 Hz, 1H), 2.53 (ddd, *J* = 13.4, 12.4 and 2.8 Hz, 1H), 2.99 (t, *J* = 9.2 Hz, 1H), 3.32–3.38 (m, 1H), 3.93 (dd, *J* = 13.6 and 2.6 Hz, 1H), 4.03 (t, *J* = 8.0 Hz, 1H), 4.62 (d, *J* = 14.0 Hz, 1H), 5.36 (dd, *J* = 9.4 and 8.0 Hz, 1H), 5.54 (ddd, *J* = 9.6, 9.2 and 7.2 Hz, 1H), 8.36 and 8.44 (2d, *J* = 5.1 Hz, 2H, H-*β*), 8.48 (s, 2H, H-*β*), 8.70 and 8.73 (2d, *J* = 5.1 Hz, 2H, H-*β*) ppm. **HRMS (ESI)** *m*/*z*: $[M + H]^+$ Calculated for $C_{49}H_{20}F_{20}N_5S^+$ 1090.112 Da; found 1090.111 Da.

Bisadduct. The UV-Vis spectrum of the bisadduct (Fig. S22†) confirms the presence of isobacteriochlorin derivatives, displaying spectral features identical to those reported in the literature.[29]

Singlet oxygen assay

The ability of the newly synthesized chlorins to generate singlet oxygen ($^1O_2$) was determined by measuring the absorbance decay of 1,3-diphenylisobenzofuran (DPiBF), a singlet oxygen quencher. To do so, stock solutions using 1.5 mg of the photosensitizers (**TPP**, **Chlor-SH_*trans*** and **Chlor-CSH_*trans***) in 5 mL of DMF were prepared. In a similar way, the stock solution of DPiBF was prepared by dissolving 1.5 mg of DPiBF in 5 mL of DMF. The final sample solutions were prepared by mixing 250 μL of DPiBF with 5 μL of the sample and adjusting the final volume to 5 mL with DMF. For the singlet oxygen measurements, one half of each final solution was kept in the dark while the other half was exposed to an irradiance of 3.6 mW cm^{-2} from a 650 nm diode laser. Each irradiance experiment took place for a total of 5 minutes, in cycles of 30 seconds of irradiance time followed by absorbance reading at 415 nm.

Photostability assay

To assess the photostability, solutions of chlorins in DMF with an absorbance of approximately 1 at the Soret band (around 400 nm) were exposed to an irradiance of 40 mW cm^{-2} from a halogen lamp for 30 minutes. Absorption spectra were collected at 5-minute intervals to evaluate the integrity of the chlorins.

DFT calculations

The structure, conformation, properties and reactivity of the newly synthesized chlorins were investigated by DFT calculations, using the M06-L[45] functional and the 6-311G(d,p)[46] basis set, as implemented in the Gaussian 16 program package.[47] Both singlet and triplet spin states were considered. The effects of DMF, chlorobenzene and chloroform solvents were included by using the PCM[48] implicit method. Vibrational frequency calculations, within the harmonic approximation, were performed to ensure that each optimized geometry corresponded to an energy minimum and to obtain the relative standard Gibbs free energy values. The Gibbs free energy of formation was calculated in the reaction solvent using one of the following equations:

$$\Delta G_f^\circ = \left(\sum G^\circ_{\text{Products}} - \sum G^\circ_{\text{Reagents}}\right) \times 627.5 \times 4.184 \quad (1)$$

$$\Delta G_f^\circ = \Delta G^\circ_{f\ \text{Azomethine ylide}} + \Delta G^\circ_{f\ \text{1,3-DC}} + \Delta G^\circ_{f\ \text{2nd ring}} \quad (2)$$

$$\Delta G_f^\circ = \left(G^\circ_{\text{Triplet State}} - G^\circ_{\text{Singlet State}}\right) \times 27.21 \quad (3)$$

where G° is the Gibbs free energy in Hartree, 627.5 × 4.184 is the conversion from Hartree to kJ mol^{-1} and 27.21 is the conversion from Hartree to eV.

^{1}H and ^{13}C NMR chemical shift values were calculated in chloroform solvent by using tetramethylsilane as the standard through the following equations:

$$CS(Hx) = \sigma(H_{TMS}) - \sigma(H_X) \quad (4)$$

$$CS(Cx) = \sigma(C_{TMS}) - \sigma(C_X) \quad (5)$$

where H_X or Cx represents one hydrogen or carbon atom and the isotropic shielding (σ) of the six equivalent hydrogen atoms, H_{TMS}, or of the four equivalent carbon atoms, C_{TMS}, of TMS has been computed using the same methodology.

The reaction kinetics of **Chlor-SH** was investigated by monitoring the 1,3-DC reaction, and the quadratic synchronous transit guided quasi-Newton method[49] was used to find transition-state structures, corresponding to a first-order saddle point.

The S_n–T_m energy gaps were calculated considering the vertical energies of both singlet and triplet states, using the TDA-TDDFT approach. Spin–orbit matrix elements were calculated with the Orca 6.0.0 program package,[50] using the triplet state optimized structure and the M06L[45] functional with the relativistic ZORA basis sets (ZORA-DEF2-SVP).[51] Spin–orbit couplings (SOCs) were calculated according to the following formula:

$$SOC_{ij} = \sqrt{\sum_n \left|\left\langle \psi_{S_i} \middle| \hat{H}_{S_0} \middle| \psi_{T_{j,n}} \right\rangle\right|^2};\ n = x, y, z \quad (6)$$

Further computational details and the cartesian coordinates of the optimized geometries are reported in the ESI.†

Conclusions

Two novel sulphur-containing pyrrolidine-fused chlorins, **Chlor-SH_*trans*** and **Chlor-CSH_*trans***, were successfully synthesized *via* a 1,3-dipolar cycloaddition reaction. In these reactions, azomethine ylides were generated *in situ* through the condensation of paraformaldehyde with cysteine or L-thiazolidine-4-carboxylic acid (for **Chlor-SH_*trans***) and homocysteine (for **Chlor-CSH_*trans***).

Due to the planar geometry of the porphyrin ring system, the azomethine ylides can adopt either *endo* or *exo* orientations during cycloaddition, resulting in the formation of *trans* and *cis* stereoisomers. Theoretical calculations indicated

Open Access Article. Published on 10 iyul 2025. Downloaded on 06.02.2026 22:33:51. This article is licensed under a Creative Commons Attribution 3.0 Unported Licence.

that the *trans* isomer exhibits greater thermodynamic stability for both synthesized chlorins, **Chlor-SH_*trans*** and **Chlor-CSH_*trans***. This finding is consistent with experimental ^{1}H NMR data, which identified the *trans* isomer as the main isolated product.

Theoretical studies showed how the formation of the second ring can occur spontaneously by reacting with another formaldehyde molecule. Furthermore, the possibility of three different products from the reaction of the amino acid used with formaldehyde provided an explanation for the lower yield obtained, since the 1,3-dipolar species formation is not spontaneous. Kinetic studies allowed for a better comprehension of the reaction with the 1,3-dipolar species. By comparing the formation energy of **Chlor-SH_*trans*** and **Chlor-CSH_*trans***, it is possible to conclude that **Chlor-CSH_*trans*** is much more stable, possibly due to the formation of the six-membered ring, which translates into a higher product yield.

Notably, **Chlor-SH_*trans*** demonstrated a higher singlet oxygen production, which can be attributed to its enhanced triplet-state stability and higher spin–orbit coupling (SOC) values. Both chlorins exhibited promising photophysical properties, including strong absorption around 650 nm, absence of aggregation and no photodegradation at the tested concentrations, suggesting strong potential for applications in photodynamic therapy (PDT).

Author contributions

J. M. and J. A. synthesized and structurally characterized all compounds and performed all experimental measurements. T. M. R. and T. E. C. M. developed the experimental setup for singlet oxygen and photostability measurements and analysed the physicochemical data. V. B. performed the spin–orbit coupling (SOC) calculations. G. B. completed the theoretical studies and supervised the manuscript content. A. M. G. S. conceived and supervised the synthetic work and manuscript writing. All authors participated in discussions, writing, and critical review of the manuscript.

Conflicts of interest

There are no conflicts to declare.

Data availability

The data supporting this article have been included as part of the ESI.†

Acknowledgements

This work received financial support from the PT national funds (FCT/MCTES, Fundação para a Ciência e Tecnologia and Ministério da Ciência, Tecnologia e Ensino Superior) through the project UID/50006 -Laboratório Associado para a Química Verde - Tecnologias e Processos Limpos. Juliana Machado thanks the University of Palermo for funding the Ph.D. project (PJ_DR_INCR10) in cotutelle with the University of Porto. The research team would like to thank the valuable contribution and support of Eulália Pereira, Miguel Peixoto de Almeida and Maria Enea. We would also like to thank the Research Center in Chemistry of the University of Porto (CIQUP) for the access to the absolute luminescence quantum yield spectrometer (Quantaurus-QY C11347-11 spectrometer). This work was additionally supported by FCT and IFIMUP grants UIDB/04968/2025 and UIDP/04968/2025.

References

1 S. Kwiatkowski, B. Knap, D. Przystupski, J. Saczko, E. Kędzierska, K. Knap-Czop, J. Kotlińska, O. Michel, K. Kotowski and J. Kulbacka, Photodynamic therapy – mechanisms, photosensitizers and combinations, *Biomed. Pharmacother.*, 2018, **106**, 1098–1107.
2 W. Jiang, M. Liang, Q. Lei, G. Li and S. Wu, The Current Status of Photodynamic Therapy in Cancer Treatment, *Cancers*, 2023, **15**, 585.
3 K. Nguyen and A. Khachemoune, An update on topical photodynamic therapy for clinical dermatologists, *J. Dermatol. Treat.*, 2019, **30**, 732–744.
4 W. M. Alshehri, B. O. AlAhmadi, F. Alhumaid, M. S. Khoshhal, Z. Y. Khawaji, H. AlHabuobi, A. M. Alosaimi, A. Alkhathami and J. Alorainy, Safety and Efficacy of Photodynamic Therapy in the Treatment of Circumscribed Choroidal Hemangioma: A Systematic Review, *Cureus*, 2023, **15**, 50461.
5 M. Nie, P. Zhang, J. L. Pathak, X. Wang, Y. Wu, J. Yang and Y. Shen, Photodynamic therapy in periodontitis: A narrative review, *Photodermatol., Photoimmunol. Photomed.*, 2024, **40**, 12946.
6 X. Hu, H. Zhang, Y. Wang, B.-C. Shiu, J.-H. Lin, S. Zhang, C.-W. Lou and T.-T. Li, Synergistic antibacterial strategy based on photodynamic therapy: Progress and perspectives, *Chem. Eng. J.*, 2022, **450**, 138129.
7 P. C. V. Conrado, K. M. Sakita, G. S. Arita, C. B. Galinari, R. S. Gonçalves, L. D. G. Lopes, M. V. C. Lonardoni, J. J. V. Teixeira, P. S. Bonfim-Mendonça and E. S. Kioshima, A systematic review of photodynamic therapy as an antiviral treatment: Potential guidance for dealing with SARS-CoV-2, *Photodiagn. Photodyn. Ther.*, 2021, **34**, 102221.
8 B. W. Henderson and D. A. Bellnier, in *Ciba Foundation symposium*, 2007, vol. 146, pp. 112–130.
9 N. V. Stepanova, L. V. Zhorina and E. B. Chernyaeva, Likely Mechanism of the Hydrophobic Sensitizer Accumulation in Tumor Cells: Mathematical Models, *Photochem. Photobiol.*, 1996, **64**, 832–837.
10 V. Zenzen and H. Zankl, Protoporphyrin IX-accumulation in human tumor cells following topical ALA- and h-ALA-application in vivo, *Cancer Lett.*, 2003, **202**, 35–42.

 This journal is © The Royal Society of Chemistry 2025

Open Access Article. Published on 10 iyul 2025. Downloaded on 06.02.2026 22:33:51. This article is licensed under a Creative Commons Attribution 3.0 Unported Licence.

11 C. J. H. Ho, G. Balasundaram, W. Driessen, R. McLaren, C. L. Wong, U. S. Dinish, A. B. E. Attia, V. Ntziachristos and M. Olivo, Multifunctional Photosensitizer-Based Contrast Agents for Photoacoustic Imaging, *Sci. Rep.*, 2014, **4**, 5342.
12 A.-G. Niculescu and A. M. Grumezescu, Photodynamic Therapy—An Up-to-Date Review, *Appl. Sci.*, 2021, **11**, 3626.
13 C. A. Robertson, D. H. Evans and H. Abrahamse, Photodynamic therapy (PDT): A short review on cellular mechanisms and cancer research applications for PDT, *J. Photochem. Photobiol., B*, 2009, **96**, 1–8.
14 J. M. Dabrowski and L. G. Arnaut, Photodynamic therapy (PDT) of cancer: from local to systemic treatment, *Photochem. Photobiol. Sci.*, 2015, **14**, 1765–1780.
15 E. A. Giuliano, J. Ota and S. A. Tucker, Photodynamic therapy: basic principles and potential uses for the veterinary ophthalmologist, *Vet. Ophthalmol.*, 2007, **10**, 337–343.
16 D. K. Chatterjee, L. S. Fong and Y. Zhang, Nanoparticles in photodynamic therapy: An emerging paradigm, *Adv. Drug Delivery Rev.*, 2008, **60**, 1627–1637.
17 P. De Silva, M. A. Saad, H. C. Thomsen, S. Bano, S. Ashraf and T. Hasan, Photodynamic therapy, priming and optical imaging: Potential co-conspirators in treatment design and optimization—a Thomas Dougherty Award for Excellence in PDT paper, *J. Porphyrins Phthalocyanines*, 2020, **24**, 1320–1360.
18 L. B. Josefsen and R. W. Boyle, Photodynamic Therapy and the Development of Metal-Based Photosensitisers, *Met.-Based Drugs*, 2008, **2008**, 1–23.
19 D. Bechet, P. Couleaud, C. Frochot, M.-L. Viriot, F. Guillemin and M. Barberi-Heyob, Nanoparticles as vehicles for delivery of photodynamic therapy agents, *Trends Biotechnol.*, 2008, **26**, 612–621.
20 R. R. Allison, G. H. Downie, R. Cuenca, X.-H. Hu, C. J. Childs and C. H. Sibata, Photosensitizers in clinical PDT, *Photodiagn. Photodyn. Ther.*, 2004, **1**, 27–42.
21 G. Shi, S. Monro, R. Hennigar, J. Colpitts, J. Fong, K. Kasimova, H. Yin, R. DeCoste, C. Spencer, L. Chamberlain, A. Mandel, L. Lilge and S. A. McFarland, Ru(II) dyads derived from α-oligothiophenes: A new class of potent and versatile photosensitizers for PDT, *Coord. Chem. Rev.*, 2015, **282–283**, 127–138.
22 S. A. McFarland, A. Mandel, R. Dumoulin-White and G. Gasser, Metal-based photosensitizers for photodynamic therapy: the future of multimodal oncology, *Curr. Opin. Chem. Biol.*, 2020, **56**, 23–27.
23 V. F. Otvagin, N. S. Kuzmina, E. S. Kudriashova, A. V. Nyuchev, A. E. Gavryushin and A. Yu, Fedorov, Conjugates of Porphyrinoid-Based Photosensitizers with Cytotoxic Drugs: Current Progress and Future Directions toward Selective Photodynamic Therapy, *J. Med. Chem.*, 2022, **65**, 1695–1734.
24 M. Prejanò, M. E. Alberto, B. C. De Simone, T. Marino, M. Toscano and N. Russo, Sulphur- and Selenium-for-Oxygen Replacement as a Strategy to Obtain Dual Type I/Type II Photosensitizers for Photodynamic Therapy, *Molecules*, 2023, **28**, 3153.
25 S. Tong, Y. Cheng, H. Liu, Y. Pang, X. Lin, Z. Hu and F. Wu, Thionation of conjugated porphyrin with enhanced photodynamic and photothermal effects for cancer therapy, *J. Photochem. Photobiol., A*, 2025, **459**, 116085.
26 J. Tang, L. Wang, A. Loredo, C. Cole and H. Xiao, Single-atom replacement as a general approach towards visible-light/near-infrared heavy-atom-free photosensitizers for photodynamic therapy, *Chem. Sci.*, 2020, **11**, 6701–6708.
27 J. W. Foley, X. Song, T. N. Demidova, F. Jilal and M. R. Hamblin, Synthesis and Properties of Benzo[a]phenoxazinium Chalcogen Analogues as Novel Broad-Spectrum Antimicrobial Photosensitizers, *J. Med. Chem.*, 2006, **49**, 5291–5299.
28 A. M. G. Silva, A. C. Tomé, M. G. P. M. S. Neves, J. A. S. Cavaleiro and C. O. Kappe, Porphyrins in Diels–Alder reactions. Improvements on the synthesis of barrelene-fused chlorins using microwave irradiation, *Tetrahedron Lett.*, 2005, **46**, 4723–4726.
29 A. M. G. Silva, A. C. Tomé, M. G. P. M. S. Neves, A. M. S. Silva and J. A. S. Cavaleiro, 1,3-Dipolar Cycloaddition Reactions of Porphyrins with Azomethine Ylides, *J. Org. Chem.*, 2005, **70**, 2306–2314.
30 A. M. G. Silva, P. S. S. Lacerda, A. C. Tomé, M. G. P. M. S. Neves, A. M. S. Silva, J. A. S. Cavaleiro, E. A. Makarova and E. A. Lukyanets, Porphyrins in 1,3-Dipolar Cycloaddition Reactions. Synthesis of New Porphyrin–Chlorin and Porphyrin–Tetraazachlorin Dyads, *J. Org. Chem.*, 2006, **71**, 8352–8356.
31 Y. Ning, Y.-W. Liu, Z.-S. Yang, Y. Yao, L. Kang, J. L. Sessler and J.-L. Zhang, Split and Use: Structural Isomers for Diagnosis and Therapy, *J. Am. Chem. Soc.*, 2020, **142**, 6761–6768.
32 N. M. M. Moura, C. J. P. Monteiro, A. C. Tomé, M. G. P. M. S. Neves and J. A. S. Cavaleiro, Synthesis of chlorins and bacteriochlorins from cycloaddition reactions with porphyrins, *ARKIVOC*, 2022, **2022**, 54–98.
33 P. B. Momo, C. Pavani, M. S. Baptista, T. J. Brocksom and K. T. Oliveira, Chemical Transformations and Photophysical Properties of *meso* –Tetrathienyl–Substituted Porphyrin Derivatives, *Eur. J. Org. Chem.*, 2014, **2014**, 4536–4547.
34 J. Almeida, A. C. Tomé, M. Rangel and A. M. G. Silva, Microwave-Assisted Synthesis and Spectral Properties of Pyrrolidine-Fused Chlorin Derivatives, *Molecules*, 2023, **28**, 3833.
35 J. Gonzales, N. V. S. D. K. Bhupathiraju, D. Hart, M. Yuen, M. P. Sifuentes, B. Samarxhiu, M. Maranan, N. Berisha, J. Batteas and C. M. Drain, One-Pot Synthesis of Four Chlorin Derivatives by a Divergent Ylide, *J. Org. Chem.*, 2018, **83**, 6307–6314.
36 J. J. A. G. Kamps, R. J. Hopkinson, C. J. Schofield and T. D. W. Claridge, How formaldehyde reacts with amino acids, *Commun. Chem.*, 2019, **2**, 126.
37 S. Kobayashi and K. A. Jørgensen, *Cycloaddition Reactions in Organic Synthesis*, Wiley, 2001.

Open Access Article. Published on 10 iyul 2025. Downloaded on 06.02.2026 22:33:51.
This article is licensed under a Creative Commons Attribution 3.0 Unported Licence.

38 V. Butera, G. Mazzone and H. Detz, Dinuclear Ruthenium (II)–Pyrrolide Complexes Linked by Different Organic Units as PDT Photosensitizers: Computational Study of the Linker Influence on the Photophysical Properties*, *ChemPhotoChem*, 2022, **6**, e202200094.

39 T. G. Mayerhöfer, A. V. Pipa and J. Popp, Beer's Law–Why Integrated Absorbance Depends Linearly on Concentration, *ChemPhysChem*, 2019, **20**, 2748–2753.

40 F. A. B. dos Santos, A. F. Uchoa, M. S. Baptista, Y. Iamamoto, O. A. Serra, T. J. Brocksom and K. T. de Oliveira, Synthesis of functionalized chlorins sterically-prevented from self-aggregation, *Dyes Pigm.*, 2013, **99**, 402–411.

41 A. F. Uchoa, K. T. de Oliveira, M. S. Baptista, A. J. Bortoluzzi, Y. Iamamoto and O. A. Serra, Chlorin Photosensitizers Sterically Designed To Prevent Self-Aggregation, *J. Org. Chem.*, 2011, **76**, 8824–8832.

42 T. Entradas, S. Waldron and M. Volk, The detection sensitivity of commonly used singlet oxygen probes in aqueous environments, *J. Photochem. Photobiol., B*, 2020, **204**, 111787.

43 N. M. M. Moura, X. Moreira, E. S. Da Silva, J. L. Faria, M. G. P. M. S. Neves, A. Almeida, M. A. F. Faustino and A. T. P. C. Gomes, Efficient Strategies to Use β-Cationic Porphyrin-Imidazolium Derivatives in the Photoinactivation of Methicillin-Resistant Staphylococcus aureus, *Int. J. Mol. Sci.*, 2023, **24**, 15970.

44 A. M. d'A. R. Gonsalves, J. M. T. B. Varejão and M. M. Pereira, Some new aspects related to the synthesis of meso –substituted porphyrins, *J. Heterocycl. Chem.*, 1991, **28**, 635–640.

45 Y. Zhao and D. G. Truhlar, A new local density functional for main-group thermochemistry, transition metal bonding, thermochemical kinetics, and noncovalent interactions, *J. Chem. Phys.*, 2006, **125**, 194101.

46 R. Krishnan, J. S. Binkley, R. Seeger and J. A. Pople, Self-consistent molecular orbital methods. XX. A basis set for correlated wave functions, *J. Chem. Phys.*, 1980, **72**, 650–654.

47 M. J. Frisch, G. W. Trucks, H. B. Schlegel, G. E. Scuseria, M. A. Robb, J. R. Cheeseman, G. Scalmani, V. Barone, G. A. Petersson, H. Nakatsuji, X. Li, M. Caricato, A. V. Marenich, J. Bloino, B. G. Janesko, R. Gomperts, B. Mennucci, H. P. Hratchian, J. V. Ortiz, A. F. Izmaylov, J. L. Sonnenberg, D. Williams-Young, F. Ding, F. Lipparini, F. Egidi, J. Goings, B. Peng, A. Petrone, T. Henderson, D. Ranasinghe, V. G. Zakrzewski, J. Gao, N. Rega, G. Zheng, W. Liang, M. Hada, M. Ehara, K. Toyota, R. Fukuda, J. Hasegawa, M. Ishida, T. Nakajima, Y. Honda, O. Kitao, H. Nakai, T. Vreven, K. Throssell Jr., J. A. Montgomery, J. E. Peralta, F. Ogliaro, M. J. Bearpark, J. J. Heyd, E. N. Brothers, K. N. Kudin, V. N. Staroverov, T. A. Keith, R. Kobayashi, J. Normand, K. Raghavachari, A. P. Rendell, J. C. Burant, S. S. Iyengar, J. Tomasi, M. Cossi, J. M. Millam, M. Klene, C. Adamo, R. Cammi, J. W. Ochterski, R. L. Martin, K. Morokuma, O. Farkas, J. B. Foresman and D. J. Fox, *Revision C.016*, 2019, preprint.

48 J. Tomasi, B. Mennucci and R. Cammi, Quantum Mechanical Continuum Solvation Models, *Chem. Rev.*, 2005, **105**, 2999–3094.

49 C. Peng and H. B. Schlegel, Combining Synchronous Transit and Quasi–Newton Methods to Find Transition States, *Isr. J. Chem.*, 1993, **33**, 449–454.

50 F. Neese, The ORCA program system, *Wiley Interdiscip. Rev.: Comput. Mol. Sci.*, 2012, **2**, 73–78.

51 E. van Lenthe, J. G. Snijders and E. J. Baerends, The zero-order regular approximation for relativistic effects: The effect of spin–orbit coupling in closed shell molecules, *J. Chem. Phys.*, 1996, **105**, 6505–6516.

This journal is © The Royal Society of Chemistry 2025